

Stochastic propagators for multi-pion correlation functions in lattice QCD with GPUs

Joel Giedt* and Dean Howarth†

*Department of Physics, Applied Physics and Astronomy,
Rensselaer Polytechnic Institute, 110 8th Street, Troy NY 12065 USA*

(Dated: August 11, 2014)

Abstract

Motivated by the application of Lüscher’s finite volume method to the study of the lightest scalar resonance in the $\pi\pi \rightarrow \pi\pi$ isoscalar channel, in this article we describe our studies of multi-pion correlation functions computed using stochastic propagators in quenched lattice QCD, harnessing GPUs for acceleration. We consider two methods for constructing the correlation functions. One “outer product” approach becomes quite expensive at large lattice extent L , having an $\mathcal{O}(L^7)$ scaling. The other “stochastic operator” approach scales as $\mathcal{O}(N_r^2 L^4)$, where N_r is the number of random sources. It would become more efficient if variance reduction techniques are used and the volume is fairly large. It is also found that correlations between stochastic propagators appearing in the same diagram, when a single set of random source vectors is used, lead to much larger errors than if separate random sources are used for each propagator. The calculations involve states with quantum numbers of the vacuum, so all-to-all propagators must be computed. For this reason, GPUs are ideally suited to accelerating the calculation. For this work we have integrated the Columbia Physics System (CPS) and QUDA GPU inversion library, in the case of clover fermions. Finally, we show that the completely quark disconnected diagram is crucial to the results, and that neglecting it would lead to answers which are far from the true value for the effective mass in this channel. This is unfortunate, because as we also show, this diagram has very large errors, and in fact dominates the error budget.

PACS numbers: 11.15.Ha, 12.38.Gc, 14.40.Be, 02.50.Fz

* giedtj@rpi.edu

† dmhowarth26@gmail.com

I. MOTIVATION

There are several reasons to attempt a study of scalar resonances in lattice gauge theory of QCD and QCD-like theories. For one, some researchers have proposed that the Higgs boson discovered at the LHC is an “imposter” [1], actually a composite state of a new strong interaction that breaks electroweak symmetry—i.e., technicolor. Of course the idea of a light composite Higgs boson has been around for some time; see for instance [2]. For this to be the case, the scalar must be surprisingly light given that the fundamental scale of techni-hadrons is $4\pi f_\pi$, where $f_\pi = v = 246$ GeV in the simplest implementation. This is achieved in two ways in the current proposals. First, there is a suppression of the dynamical mass because the lightest scalar is a techni-dilaton,¹ the state that would become massless when scale invariance is restored at the edge of the conformal window. Second, there is a correction, principally due to the top quark, which leads to an “electroweak” subtraction to the mass [4]. These two effects are then argued to make possible the mass of 125 GeV. To put this on firm ground, it is necessary to verify on the lattice that the suppression of the dynamical mass really occurs in the vicinity of the lower edge of the conformal window. For this, we must measure the mass of the techni- σ , the lightest scalar state.

Another motivation is to better understand the somewhat controversial σ , or $f_0(500)$, resonance of QCD. This is a very broad state, so broad that it is difficult to resolve it from scattering data. It cannot be described by a Breit-Wigner peak, and is difficult to distinguish from a smoothly varying background. Theoretical evidence for this resonance, obtained by a first principles method (lattice QCD) would be welcome in helping to resolve the controversy. In particular, if the mass and width computed from the lattice agrees with determinations from experimental data, it would be further evidence for the existence of this state.

Apart from the existence of the σ state, it is also of interest to understand its composition at the partonic level, which can be mapped onto the linear combination of local operators that should be used to create the state from the vacuum, without contamination from other states; i.e, the “eigen-operator,” as would appear in a variational analysis with a complete operator basis. For instance, the mesonic operator $\bar{q}q$ can mix with the gluonic operator $\text{Tr } F_{\mu\nu}F_{\mu\nu}$. This suggests that the σ will actually be superposition of mesonic and glueball

¹ See the recent review [3] and references therein.

states. It would be very interesting to obtain from the lattice an estimate of the relative contributions of these two types of states. It has also been proposed [5, 6] that the σ (and other scalars) may be predominantly a tetraquark state $q^2\bar{q}^2$. Of course there are a couple of ways to form a color singlet in such a four-quark state (it could be molecular $(q\bar{q})(q\bar{q})$ or truly tetraquark where the colors are all tangled up), so here again is a question about the internal structure at the partonic level. This can be addressed using lattice QCD by evaluating the different overlaps (matrix elements) of various interpolating operators, $\langle 0|\mathcal{O}_i(0)|\sigma\rangle$. The composition of the σ in terms of these possibilities will affect its decays and interactions, and so they are important for understanding the properties of this lightest non-Nambu-Goldstone boson state of QCD.

It is also worth remarking that the sigma state is interesting from the perspective of chiral symmetry in QCD. Indeed, in the linear representation, the sigma is the chiral partner of the pions. However, its properties are radically different from pions, revealing the large effects of spontaneous chiral symmetry breaking. There have been a number of lattice studies of the scalar resonances in QCD, which we will touch upon below in Section III.

We now summarize the content of the remainder of this article. Our main results will be on a preliminary calculation of the multipion correlation function with an overlap on the $I = 0, 0^{++}$ channel, corresponding to $\pi^+\pi^- \rightarrow \pi^+\pi^-$. We have studied approaches involving stochastic propagators and the associated errors, by comparing to exact point source calculations on small lattices. We also have conducted this exploratory work in order to better understand the relative contributions of different contractions of the quark fields, and to identify the largest sources of error, in the hope of developing superior strategies going forward. However, before coming to these results, we first explain various foundational material that will fit into our larger program which we are initiating with this work. In Section II we explain why multipion correlation functions are of interest in trying to study the σ resonance on the lattice. Next in Section III we quickly survey previous lattice studies of the sigma, mentioning some of the different approaches and interpretations. It will be seen that there is not complete consensus, and that there is still quite a bit of room for progress in this area. All of the approaches surveyed there involve using interpolating operators for the sigma, with different supposed contents for this state, followed by various standard approaches involving exponential decays of correlation functions. However, some concerns have been raised about this entire approach for a particle with open decay channels [7–9].

The approach that we will therefore advocate, and which is our eventual goal, is described next in Section IV. This avoids the difficulties associated with the locations of poles on a finite lattice, by accessing the resonance indirectly through a lattice analysis of $\pi^+\pi^- \rightarrow \pi^+\pi^-$ scattering using finite volume effects. It is precisely for this type of study that we need the multipion correlation functions which are the subject of our exploratory investigations toward the end of this article. Thus we provide a brief review of Lüscher's method, and then discuss how it should be applied in the case of the σ , which is a very broad resonance. We will point out that there are reasonably reliable methods which have been used for extracting resonance information from the experimental scattering phase shift data. These methods can also be used for interpreting the results of the Lüscher type approach. A summary of the contractions that occur in the multipion correlation function, represented by diagrams, is given in Section V. Some remarks about momentum eigenstates of pions versus Fourier transformed operators are made, making the point that these are not exactly the same thing in a multipion correlation function, due to interactions.

Section VI is intended mainly by way of review, since it summarizes the approach of trying to construct a reasonable basis of interpolating operators for the σ , which would then be used for the extraction of its properties from correlation functions using a variational analysis. We will not study all of these operators and correlation operators in this paper, nor will we implement a variational analysis. Our goal instead is to study aspects of the multipion correlation functions that would be involved in the Lüscher type analysis. However, we do envision implementing an analysis of the type described in Section VI at a later point, and in this case the stochastic methods which are the subject of our analysis in later sections will be used due to the presence of quark-disconnected diagrams in either approach. In particular, the approach of Section VI has one advantage over the Lüscher approach described in Section IV: using the variational technique, one can obtain results for the composition of the σ state in terms of quarks and gluons. We describe this feature in our brief review in Section VI, but leave its implementation to a future study.

Various ways to use the stochastic propagators in our calculations are described in Section VII. This is where some of our main results are given. We describe in particular the advantages of using independent random sources for each propagator appearing in a diagram, and demonstrate that this results in a much reduced error. To obtain these results we have compared to the rather expensive calculation of computing the full all-to-all propagator

using point sources. This is only possible on the very small volumes ($4^3 \times 8$) on which we work in this exploratory study. Thus our goal in this paper is not to obtain physical results, but rather to study technical issues of computing the diagrams, controlling errors, and the relative weights of the different diagrams. We also show that the outer product operation involved in filling in the stochastic operators from the solution vectors and source vectors quickly becomes more expensive than the actual inversions as the system size is increased. For this, we provide timing benchmarks, using GPU acceleration of the inversion. We then show the GPU acceleration of this fill operation in our subsequent code which we have developed. The L^7 scaling of the fill operation (outer product) is then contrasted to another approach which avoids the outer product by using “stochastic operators.” It scales like $N_r^2 \times L^4$, which does not grow with lattice size in the same very unfortunate way. However, in the absence of variance reduction, we find through our analysis that N_r , the number of random sources, must be very large. In order to keep stochastic errors under control, we have found it necessary to take $N_r = 10^3$. Thus the stochastic operator approach is enormously expensive for the small volumes on which we work. We are then able to argue that the outer product method should be used on volumes less than $L = 22$, but that for larger volumes, dilution and the stochastic operator approach should be used. In this way our exploratory study described in this paper sets the stage for larger scale calculation that will ultimately lead to physical results. Clearly these issues should first be sorted out and studied thoroughly before making a large investment in computer time.

In Section VIII we describe the remainder of the diagrams in terms of quark propagators and give our results for each of them in our simulations. We fit each diagram to a cosh function and obtain effective masses in each case. The diagrams are then combined to form the total correlation function and an effective mass is then obtained for this full result. Here we are able to see that one diagram in particular, the completely quark-disconnected diagram, pulls the effective mass down and dominates the error budget. It has large vacuum subtractions, and because the two pieces which are being subtracted are large, the final signal-to-noise ratio is small. Nevertheless, we are able to show through our analysis that ignoring the partially disconnected and/or completely disconnected diagrams would lead to a very large error in the total effective mass. This is one of the uses of extracting the effective mass for each diagram, since one can see how they have very different effects on the final answer. Also, there is an interpretation of each diagram in terms of the states

in the intermediate channel. The fully connected diagram is sensitive to four-quark states, the partially disconnected diagram is sensitive to two-quark states, and the completely disconnected diagram is a probe of coupling to the purely gluonic states. Our analysis shows that all of these channels are playing an important role in the states created by the two pion operator, even in the quenched approximation in which we work. In particular, the nonzero result for our completely disconnected diagram shows that the four quark operator has a nonzero overlap with purely gluonic states, even in the quenched approximation. We attribute this nonorthogonality to the lack of unitarity in the quenched theory. In other words, because the quenched theory (including quarks and ghosts) is not unitary, it does not have a Hermitian Hamiltonian, and hence one should not expect orthogonality of eigenstates of the transfer matrix. In Section IX we make our conclusions and mention directions for our future work. Principally it will be to follow up our analysis on larger lattices, using the lessons that we have learned in the present study.

II. WHY MULTIHADRON CORRELATION FUNCTIONS ARE NECESSARY

Consider the σ resonance in quantum chromodynamics (QCD). It is the lightest scalar hadron with a mass of about 500 MeV, and a comparable width. It is not stable, and in particular it can decay into two pions. Therefore at the physical pion mass, simply looking for the σ in the exponential decay of the correlation function of the scalar interpolating operator $\mathcal{O}_S = \bar{q}q$ will fail:

$$C(t) = \sum_{\mathbf{p}} A_{\mathbf{p}} e^{-E_{2\pi(\mathbf{p})}t} + B e^{-m_{\sigma}t} \cos(\Gamma_{\sigma}t/2) + \dots \quad (2.1)$$

The two pion continuum will dominate because for many values of \mathbf{p} , (especially for large L) $E_{2\pi(\mathbf{p})} < m_{\sigma}$. Thus we will not be able to extract the desired signal because of the large continuum background (scattering states). The only way to overcome this is to have a method for identifying the two-pion continuum states and subtracting them off from $C(t)$ with a high degree of accuracy. We will comment on the prospects for this below. Another comment is that for a resonance with open decay channels the energy eigenvalue is complex, $E_{\sigma} = \sqrt{s} = m_{\sigma} - \frac{i}{2}\Gamma_{\sigma}$. This has been explored quite some time ago in Euclidean space in [7]. The inverse propagator of the resonance is given by

$$G^{-1}(p) = p^2 + m^2 - \Sigma(p^2) \quad (2.2)$$

Setting the spatial momentum of the resonance to zero, $\mathbf{p} = 0$, the propagator becomes simply a function of $p_0 = iE$. Since for the lattice applications we wish instead to have the time dependent Green's function, we perform the relevant Fourier transform

$$G(t) = \frac{1}{2\pi} \int_{-\infty}^{\infty} dp_0 e^{ip_0 t} G(p_0) \quad (2.3)$$

What is show in [7] is that at large times, and in the approximation that the imaginary part of the self-energy is constant, $\Gamma = \text{Im}\Sigma/m_\sigma = \text{const.}$, the behavior is

$$G(t) \approx \frac{1}{2m_\sigma} e^{-m_\sigma t} \cos(\Gamma t/2) + \frac{\Gamma}{4m_\sigma \pi (m_\sigma - 2m_\pi)^2 t} e^{-2m_\pi t} \quad (2.4)$$

One thing that we see from this analytic result is that the full complex eigenvalue of the resonance enters its time dependence, reflected in the factor $\cos(\Gamma t/2)$. We also see that the assumption that $\text{Im}\Sigma(E) = \text{const.}$ has led to the absence of the two pion states with nonzero relative momentum. In order to obtain these we would presumably also need the energy dependence of the imaginary part of the self-energy. In a finite volume, for instance L^3 in the lattice context, the momenta will be quantized but there is no reason to expect that this would cause $\text{Im}\Sigma(E)$ to vanish, so the $\cos(\Gamma t/2)$ factor should also appear there. Thus at the very least, fitting a resonance directly from an correlation function of the corresponding interpolating operator will be quite difficult and nonstandard in its time dependence. The scattering states must be subtracted; according to (2.4), they may have a time dependence which is not as simple as the one given in (2.1)—note the t^{-1} factor that appears in (2.4), which is completely unexpected from a transfer matrix manipulation involving a sum over a discrete set of states. It is unclear whether or not this t^{-1} factor depends in a crucial way on having a true continuum of states (present at $L \rightarrow \infty$). Even once the scattering states have been identified and subtracted, the $\cos(\Gamma t/2)$ factor would need to be taken into account, and this would be subject to unknown modifications given that $\text{Im}\Sigma(E)$ is not really independent of E .

A solution to this problem is to obtain the properties of the sigma particle by looking for it explicitly as a resonance in the $\pi\pi \rightarrow \pi\pi$ channel, using Lüscher's method, which is described in Section IV. It must be said that this is not easy, and in fact has only been successfully applied in channels with nonzero isospin. However, we believe that through persistent effort the difficulties can be overcome, since there is not any insurmountable obstacle, in principle.

III. PREVIOUS LATTICE STUDIES

The first study of the sigma resonance in lattice QCD was [10], in the quenched approximation. Another early quenched study was [11]. This studied the “tetraquark” possibility, i.e., that the sigma is a $q^2\bar{q}^2$ state rather than a $q\bar{q}$ state. However, they ignored the diagrams that involve all-to-all propagators, whereas we will include these below. Indeed we show that they are crucially important, and that neglecting them leads to very large errors. On the other hand, our inclusion of so-called partially disconnected diagrams (Figs. 1c and 1d) means that there will be mixing with the $q\bar{q}$ state even in the quenched approximation. So in a sense, our results are somewhat more confusing, though closer to the physical reality. Mixing with glueball states was considered in [12]. We pick up this effect through our completely disconnected diagram (Fig. 1b). A dynamical quark calculation was carried out in [13].

The work [14] studied unquenched QCD and found a resonance corresponding to the sigma. They use the interpolating operator $\bar{q}q$ and include the so-called disconnected diagrams where the quarks in the interpolating operator are contracted with each other. They find results of $m_\sigma = xm_\pi$ with $x = 1.6, 1.7$ and 1.9 in order of increasing pion mass. Since in all cases $m_\sigma < 2m_\pi$, they are able to avoid the two-pion continuum to some extent (it is basically an excited state that can in principle be avoided by going to large times). However, with $m_\sigma = 1.9m_\pi$, the suppression of the lightest two-pion continuum state is not much, and so their results will be contaminated to some degree. This highlights the necessity of approaches which address this issue, as we describe in some detail here.

Ref. [15] concerns itself with all of the f_0 states. In particular, they emphasize the effective of mixing with the lightest 0^{++} glueball state, which in quenched QCD is about 1.6 GeV. This will tend to lower the $q\bar{q}$ state compared to the quenched theory. In this work, they take into account quark-disconnected diagrams, and work in an unquenched theory. This is a follow up to their earlier effort in Ref. [13] where mixing with the gluonic states was considered in the quenched approximation, together with some unquenched results for the fermionic correlator.

Ref. [16] uses a sequential empirical Bayes method to extract several states within a correlation function. Making use of volume dependence [17], they are able to identify scattering states. They do find a state consistent with a 600 MeV σ , and which has a significant overlap

with the tetraquark interpolating operator that they use. Ref. [18] interprets these lattice results in terms of various constitutive models, tetraquark, $q\bar{q}$ and glueball, in the different energy regimes. Ref. [19] continues with this group finding support for the tetraquark model using a variational approach. A further study into the tetraquark interpretation of the sigma resonance (and other members of the scalar nonet) was investigated in [20]. Indeed, they find that the sigma has a significant tetraquark component. One thing that is particularly interesting to us about this work is that they identify the two-pion continuum states and deal with them in a rigorous way, applying the variational (generalized eigenvalue) technique. However, they neglect the so-called disconnected diagrams, something which we will not do in our study.

By contrast, Ref. [21] does not find evidence for a tetraquark state, but only a heavy (1.32 GeV) $q\bar{q}$ state. However, they do not include the quark-disconnected diagrams. Another effort to find tetraquarks is [22], again with a negative result. More recent work in this direction includes [23] where they again ignore quark-disconnected diagrams and find a negative result for the existence of tetraquark states. A more general study along these lines is [24]; however it is inconclusive, while taking into account the quark-disconnected contributions.

IV. LÜSCHER'S METHOD

In all of the applications that we envision, we will eventually work well into the chiral limit where the “pions” are light enough that $\sigma \rightarrow \pi\pi$ is kinematically allowed. As described above, this makes the extraction of the σ mass challenging, since there is a two-pion continuum in the same channel. Furthermore, there are concerns about attempting to use interpolating operators and correlation functions of the sigma, because there is an open decay channel—it has been suggested that this may lead to erroneous results because the pole in the continuum infinite volume theory is on the second Riemann sheet in the complex plane at $m_\sigma - i\Gamma_\sigma/2$, whereas on a finite lattice it has been argued that the singularities in the T matrix would be along the real axis [8]; however see [7] and comments in [9]. The trick that we intend to use to avoid these difficulties is standard to lattice quantum chromodynamics: we take advantage of finite volume to obtain the scattering phase shift $\delta(s)$ in the two-pion scalar, flavor singlet channel [25–28]. From this, there are well-known techniques

for analyzing $\delta(s)$ in order to extract resonances, and hence the mass and width of σ . The method that we will follow as our studies progress introduces a total momentum \mathbf{P} for the pion pair and has been presented originally in [29]. Some recent examples of the application of this method within QCD are [30–35].

We are interested in two pion states with total momentum

$$\mathbf{P} = \mathbf{p}_1 + \mathbf{p}_2, \quad (4.1)$$

in the flavor singlet ($I = 0$) channel. We extract the energy of these states for instance through:

$$\sum_{\mathbf{xy}} e^{i\mathbf{p}_1 \cdot \mathbf{x} + i\mathbf{p}_2 \cdot \mathbf{y}} \langle 0 | TP^+(t, \mathbf{x}) P^-(t, \mathbf{y}) P^+(0, \mathbf{0}) P^-(0, \mathbf{0}) | 0 \rangle_{\text{conn.}} \sim e^{-tE_{2\pi}} \quad (4.2)$$

Computation of this correlation function requires the evaluation of fermion “disconnected” diagrams. Fig. 1 show both the connected and disconnected pieces. The disconnected pieces do not vanish because we are in the flavor singlet channel. On the lattice of size L , the total momentum is quantized:²

$$\mathbf{P} = \mathbf{d} \frac{2\pi}{L}, \quad \mathbf{d} \in \mathbf{Z}^3 \quad (4.3)$$

The lab frame energy is related to center of mass momentum p^* through

$$E_{2\pi}^2 = \mathbf{P}^2 + 4(p^{*2} + m_\pi^2) = \mathbf{P}^2 + s \quad (4.4)$$

This defines p^* (and equivalently s) once the energy is extracted from the lattice correlation function. Related to p^* is the quantity

$$q = \frac{p^* L}{2\pi} \quad (4.5)$$

and then the phase shift can be obtained from

$$\tan(-\phi^{\mathbf{d}}(q)) = \frac{\gamma q \pi^{3/2}}{Z_{00}^{\mathbf{d}}(1; q^2)} \quad (4.6)$$

Here we have used

$$\mathbf{v} = \frac{\mathbf{P}}{E_{2\pi}}, \quad \gamma = (1 - \mathbf{v}^2)^{-1/2} \quad (4.7)$$

² More properly, the lattice momenta $\frac{2}{a} \sin(\mathbf{P}a/2)$ will appear in the dispersion relation. However, for a sufficiently small and \mathbf{P} not too large (i.e., $|\mathbf{P}a| \ll 1$), then the continuum expression is a reasonable approximation.

Recalling that s is a function of q , one has

$$\delta(s) = -\phi^{\mathbf{d}}(q) \pmod{\pi} \quad (4.8)$$

Above, the generalized zeta function is involved:

$$Z_{00}^{\mathbf{d}}(\mathbf{s}; q^2) = \frac{1}{\sqrt{4\pi}} \sum_{\mathbf{r} \in P_{\mathbf{d}}} (\mathbf{r}^2 - q^2)^{-s} \quad (4.9)$$

where

$$P_{\mathbf{d}} = \{\mathbf{r} \in \mathbf{R}^3 | \mathbf{r} = \tilde{\gamma}^{-1}(\mathbf{n} + \mathbf{d}/2), \mathbf{n} \in \mathbf{Z}^3\} \quad (4.10)$$

The notation here is that

$$\tilde{\gamma}^{-1}\mathbf{x} = \gamma^{-1}\mathbf{x}_{\parallel} + \mathbf{x}_{\perp} \quad (4.11)$$

a decomposition in terms of components parallel to the center of mass velocity and perpendicular to it.

Typically what is done next is to assume that the scattering is dominated by a single narrow resonance. Thus once the phase shift has been determined by the above formulae, one would impose the Breit-Wigner relation (e.g., used in the recent analysis [30, 31]):

$$\frac{-\sqrt{s}\Gamma(s)}{s - m_{\sigma}^2 + i\sqrt{s}\Gamma(s)} = \frac{e^{2i\delta(s)} - 1}{2i} \quad (4.12)$$

equivalent to the formula:

$$\tan \delta(s) = -\frac{\sqrt{s}\Gamma(s)}{s - m_{\sigma}^2} \quad (4.13)$$

Here the width $\Gamma(s)$ is parameterized as

$$\Gamma(s) = \frac{5p^* g_{\sigma\pi\pi}^2}{16\pi s} \quad (4.14)$$

taking into account the five channels of decay into identical bosons. This is analogous to the $\Gamma(s)$ used in other QCD analyses [36, 37]. Working on different volumes with various total momentum \mathbf{P} for the pion pair, one obtains a fit for the coupling $g_{\sigma\pi\pi}$ and the mass m_{σ} . The physical width of σ is obtained by evaluating $\Gamma_{\sigma} = \Gamma(m_{\sigma}^2)$.

However, in our case of the σ , the Breit-Wigner relation (4.12) is not appropriate. As mentioned in the introduction, the sigma resonance is very broad and is not well described by a Breit-Wigner resonance. Hence we anticipate that a fit to the formula (4.12) will not be

very successful. For the sigma what should be done instead is to mirror the recent analyses of the experimental data. In particular, once $\delta(s)$ data is obtained from the lattice, it could be fit as a function of s to each of the forms considered in [38]. Then these analytical expressions can be used to identify the pole in the scattering amplitude in the complex \sqrt{s} plane, allowing for a determination of the sigma properties. The result would be similar to [38], in that the spread across the various fitting forms would provide a systematic theoretical error. An alternative, which may lead to more precise results because of theoretical constraints, would be to analyze $\delta(s)$ using Roy equations.

V. THE TWO PION CORRELATION FUNCTION

The two-pion correlation function that we would like to compute is

$$\begin{aligned}
C(x, y, z) = & \langle 0|TP^+(y)P^-(z)P^+(x)P^-(0)|0\rangle \\
& - \langle 0|TP^+(y)P^-(z)|0\rangle\langle 0|TP^+(x)P^-(0)|0\rangle \\
& - \langle 0|TP^+(y)P^-(0)|0\rangle\langle 0|TP^-(z)P^+(x)|0\rangle
\end{aligned} \tag{5.1}$$

where we will take

$$x = (0, \mathbf{x}), \quad y = (t, \mathbf{y}), \quad z = (t, \mathbf{z}) \tag{5.2}$$

Note that we have generalized (4.2) somewhat by allowing one of the pions at the source location (timeslice $t = 0$) to have an arbitrary spatial location. This allows us to sum over this insertion and increase statistics. It also increases the overlap with the desired momentum state if we Fourier transform with respect to \mathbf{x} appropriately. Thus in general Fourier transforms are performed with respect to \mathbf{x} etc. to get momentum eigenstates for the pions. We do not need to Fourier transform the operator at the origin because it will be projected to $\mathbf{k}_4 = -(\mathbf{k}_1 + \mathbf{k}_2 + \mathbf{k}_3)$ by momentum conservation. Note also that we have subtracted off the product of single-pion correlation functions. This is not necessary, since the corresponding terms of the form $e^{-E_\pi(\mathbf{k}_1)t - E_\pi(\mathbf{k}_2)t}$ could be included in the fit, and thereby separated off to reveal the interaction energy $E_{2\pi}(\mathbf{k}_1 + \mathbf{k}_2) - E_\pi(\mathbf{k}_1)t - E_\pi(\mathbf{k}_2) \neq 0$. However, we view it as beneficial to subtract off these contributions at the very beginning in order to minimize the appearance of such terms.

One comment is in order here. Let us define the Fourier transform of the pseudoscalar operator,

$$\tilde{P}^\pm(\mathbf{p}) = \sum_{\mathbf{x}} e^{i\mathbf{p}\cdot\mathbf{x}} P^\pm(\mathbf{x}) \quad (5.3)$$

Then note that after inserting the complete set of states in the middle of the correlation function (i.e., between the operators at timeslices t and 0), one has the following matrix elements:

$$\langle 0 | \tilde{P}^+(\mathbf{p}_1) \tilde{P}^-(\mathbf{p}_2) | n \rangle \quad (5.4)$$

where $|n\rangle$ is an energy eigenstate. However, it is important to note that matrix elements will in general be nonzero if the state $|n\rangle$ has the same quantum numbers as the operator $\tilde{P}^+(\mathbf{p}_1)\tilde{P}^-(\mathbf{p}_2)$. This is a 0^{++} operator with $I = 0$ and total momentum $\mathbf{P} = \mathbf{p}_1 + \mathbf{p}_2$. Any state with these quantum numbers will give a nonzero overlap. In particular

$$\langle 0 | \tilde{P}^+(\mathbf{p}_1) \tilde{P}^-(\mathbf{p}_2) | \pi(\mathbf{p}_1 + \mathbf{k}) \pi(\mathbf{p}_2 - \mathbf{k}) \rangle \neq 0 \quad (5.5)$$

for any momentum \mathbf{k} . Thus, not only pions of momenta \mathbf{p}_1 and \mathbf{p}_2 appear in the intermediate state. The existence of these other states will contaminate some of the results in the preceding section. However, it is reasonable to expect that the largest overlap will be with the state $|\pi(\mathbf{p}_1)\pi(\mathbf{p}_2)\rangle$, so that $\mathbf{k} = 0$ is the strongest channel. In this case, the approximation that one makes in thinking of $\tilde{P}^+(\mathbf{p}_1)\tilde{P}^-(\mathbf{p}_2)$ as creating the state $|\pi(\mathbf{p}_1)\pi(\mathbf{p}_2)\rangle$ will be a good one.

As noted above, (truly) disconnected pieces have been subtracted off from

$$\langle 0 | T P^+(y) P^-(z) P^+(x) P^-(0) | 0 \rangle$$

in order to get a connected correlation function. It will turn out that the subtraction of the disconnected pieces associated with Fig. 1b will be a significant source of error, and yet crucial to the final answer. These contributions are problematic because they involve propagators on the same timeslice, so they are large. Errors associated with the terms that are being subtracted are therefore amplified in the net result, since one has the subtraction of two large terms which are approximately equal. If we had not performed the subtraction, the fit for Fig. 1b would also require a large constant contribution. Thus we would be trying to separate off this constant and the smaller nonconstant terms would come with a large

error. So, in either case there is a large error because of the vacuum contribution to the diagram.

The relevant contractions are shown in Figs. 1a-1d, which will be referred to below as Diagrams 0 through 3. While these resemble Feynman diagrams, it should be kept in mind that these are really just quark propagators obtained in the background of the gauge field configuration. They must be averaged over all gauge field configurations weighted by $e^{-S_{\text{eff}}}$ where $S_{\text{eff}} = S_g - N_f \ln \det M$ with S_g the gauge action and M the fermion determinant; N_f is of course the number of (degenerate) flavors. In the present study we will work in the quenched approximation, where we set $N_f = 0$. One can think of this as a sum over all possible gluon insertions into the diagrams in Fig. 1, but this is also inaccurate since perturbation theory is an asymptotic series, which does not converge when “all orders” are included—at least in the continuum in infinite volume.

Nevertheless dressing the diagrams can be helpful intuitively. One then sees that Diagram 0, Fig. 1a, has in its intermediate state four-quark contributions. Thus this part of the correlation function is sensitive to the tetraquark $qq\bar{q}\bar{q}$ and the molecule $q\bar{q}q\bar{q}$. Diagram 1, Fig. 1b, has only gluons in its intermediate state (imagine a vertical line separating the left and right hand sides), and so it is sensitive to the glueball contribution in the decay of the correlation function. Diagrams 2 and 3, Figs. 1c-d, have two-quark intermediate states, so they are sensitive to the $q\bar{q}$ contribution. These statements are all valid in the quenched approximation. However, if the effects of the fermion determinant were included, then fermion loops would appear. Then the diagrams cannot be so cleanly separated in terms of intermediate state contributions. For example, if a fermion loop is added to Diagrams 2 and 3, then four-quark states appear. From this perspective, it is interesting to consider the quenched approximation as a probe of the content of the σ state, even though it is unphysical due to the lack of unitarity.

VI. INTERPOLATING OPERATORS FOR THE σ

As mentioned in Section I above, this section is intended mainly as a review of the primary approach which has been used on the lattice for studying the properties of the σ resonance. It comes, however, with the reservations expressed in [7–9]. It has the advantage of being able to analyze the content of the σ state in terms of quarks and gluons, something which

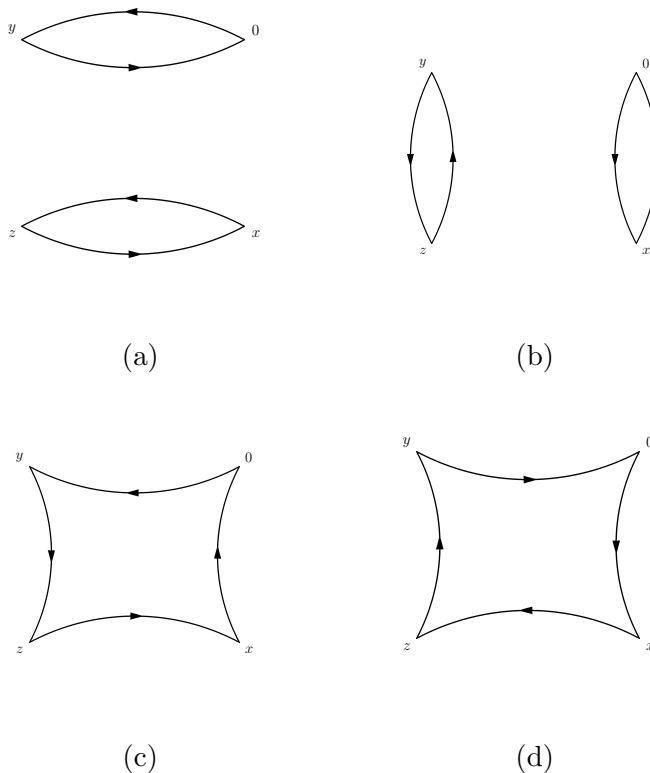


FIG. 1. The four types of contractions of the quark fields that we can have. These propagators are then averaged over the gauge field configurations to get the correlation function.

the Lüscher approach that we described above will not do. Although we have promoted the Lüscher method above, it can be seen from the studies surveyed in Section III above that one should not completely give up on the more direct method of evaluating correlation functions of the interpolating operators for the σ . For one, it is possible to study the theory at heavy pion masses where $\sigma \rightarrow \pi\pi$ cannot occur. For two, it may be possible to subtract off the two-pion continuum for lighter pion masses. To see this, note that the correlation function can be represented as

$$C(t) = \sum_n A_n e^{-E_n t} \quad (6.1)$$

On the other hand, by straightforward arguments we see that in finite volume L^3 , the coefficients scale with volume [17]

$$A_n^{1\text{-particle}} \sim 1, \quad A_n^{2\text{-particle}} \sim \frac{1}{L^3} \quad (6.2)$$

since they represent the modulus squared of what is essentially a wavefunction for a given state: $A_n = |\langle 0|\mathcal{O}(0)|n\rangle|^2$ and there is an L^3 factor coming from the Fourier transform with respect to \mathbf{x} . Thus by identifying the volume scaling of the coefficients, there is a hope of removing the contaminating continuum states.³ Of course variational techniques will be needed in order to deal with the multiple exponentials; or one can use the sequential empirical Bayes method [16], which requires a large number of timeslices.

For the variational method, it is important to enumerate many interpolating operators for the σ . Many options have been given in the papers reviewed in Section III above, and we merely provide a brief sketch at this point. Here $q = (u, d)$ corresponds to the two flavors of light quarks. Then there is the simplest singlet operator

$$\Phi_1 = \bar{q}q \tag{6.3}$$

Next there are molecular options

$$\Phi_2^A = \bar{q}\Gamma^A q\bar{q}\Gamma^A q \tag{6.4}$$

where Γ^A represent various combinations of Dirac gamma matrices. Finally, the tetraquark combines scalar diquarks

$$\begin{aligned} \Phi_3 &= \sum_a [ud]_a [\bar{u}\bar{d}]_a \\ [ud]_a &= \epsilon_{abc}(u^{Tb}C\gamma_5d^c - d^{Tb}C\gamma_5u^c), \quad [\bar{u}\bar{d}]_a = \epsilon_{abc}(\bar{u}^bC\gamma_5\bar{d}^{Tc} - \bar{d}^bC\gamma_5\bar{u}^{Tc}) \end{aligned} \tag{6.5}$$

Another operator that can be included is the Pauli term:

$$\Phi_4 = \bar{q}F_{\mu\nu}\sigma_{\mu\nu}q \tag{6.6}$$

since this is also 0^{++} . This would have an interpretation as a hybrid sort of state, containing at the partonic level both quarks and gluons.

Of course the list could go on *ad infinitum*, but at this point we have represented the basic classes of partonic contents, and to go beyond this set of operators would simply take us into further details of the variational approach to obtaining the ground state. So we stop at this point and merely consider the variational method with the set that we have at hand. At a first pass, one would consider the linear combination

$$\mathcal{O}_0 = \sum_i \eta_i \Phi_i \tag{6.7}$$

³ We thank Keh-Fei Liu for pointing this out to us.

compute the expectation value $C(t) = \langle \mathcal{O}_0(t) \mathcal{O}_0(0) \rangle$ and optimize the η_i to minimize the effective mass $m_{\text{eff}}(t) = -\ln[C(t+1)/C(t)]$. By slightly more sophisticated methods, i.e., the generalized eigenvalue problem, one can also obtain information about the excited states. In this approach one builds an entire matrix

$$C_{ij}(t) = \langle \Phi_i(t) \Phi_j(0) \rangle \quad (6.8)$$

and solves the linear algebra problem

$$C(t)u_n(t, t_0) = \lambda_n(t, t_0)C(t_0)u_n(t, t_0) \quad (6.9)$$

for the generalized eigenvalues $\lambda_n(t, t_0)$ and generalized eigenvectors $u_n(t, t_0)$. At large times,

$$\lambda_n(t, t_0) \approx e^{-E_n(t-t_0)} \quad (6.10)$$

so that one also gets energies of the excited states. The approximations improve as the number of operators is expanded. The eigenvectors also allow one to obtain the amplitudes of each operator in the eigenstates, as has been done in the present context in [20]. The matrix of correlation functions can be written as

$$C_{ij}(t) = \sum_n Z_i^n Z_j^{n*} e^{-E_n t}, \quad Z_i^n = \langle 0 | \Phi_i(0) | n \rangle \quad (6.11)$$

and then [39]

$$|Z_i^n| = |\langle 0 | \Phi_i(0) | n \rangle| = \frac{|\sum_k C_{ik}(t) u_k^n(t, t_0)|}{[\sum_{lm} |u_l^{n*}(t, t_0) C_{lm}(t) u_m^n(t, t_0)|]^{1/2}} e^{E_n t/2} \quad (6.12)$$

Thus we can see to what degree a particular state is $q\bar{q}$, $qq\bar{q}\bar{q}$, $q\bar{q}q\bar{q}$, $q\bar{q}gg$, etc.

There is some evidence from the lattice that at relatively heavy pion masses, $m_\sigma < 2m_\pi$, so that it is no longer a resonance, but a stable bound state. In this case one does not have to fight the two-pion continuum in extracting the σ state. This indeed seems to be the case in [20] and [14].

VII. STOCHASTIC PROPAGATORS

We have conducted studies comparing stochastic propagators to exact results using point source propagators. For instance, consider the “connected” Diagram 0, Fig. 1a, where the bottom contractions involve a source at $(0, \mathbf{x})$ and a sink at (t, \mathbf{z}) . In terms of the fermion

propagator S (inverse of the lattice fermion matrix computed in the background of the gauge fields) this diagram is equal to

$$C_0(t, \mathbf{x}, \mathbf{y}, \mathbf{z}) = \langle \text{Tr} [S(t, \mathbf{y}; 0, \mathbf{0}) S^\dagger(t, \mathbf{y}; 0, \mathbf{0})] \text{Tr} [S(t, \mathbf{z}; 0, \mathbf{0}) S^\dagger(t, \mathbf{x}; 0, \mathbf{0})] \rangle - \langle \text{Tr} [S(t, \mathbf{y}; 0, \mathbf{0}) S^\dagger(t, \mathbf{y}; 0, \mathbf{0})] \rangle \langle \text{Tr} [S(t, \mathbf{z}; 0, \mathbf{0}) S^\dagger(t, \mathbf{x}; 0, \mathbf{0})] \rangle \quad (7.1)$$

where the dagger is only w.r.t. the spin-color indices, since the site indices have already been interchanged using the γ_5 hermiticity. The average is over gauge field configurations. Since we will perform a Fourier transform

$$\sum_{\mathbf{x}, \mathbf{y}, \mathbf{z}} e^{i(\mathbf{k}_1 \cdot \mathbf{x} + \mathbf{k}_2 \cdot \mathbf{y} + \mathbf{k}_1 \cdot \mathbf{x})} C_0(t, \mathbf{x}, \mathbf{y}, \mathbf{z}) \quad (7.2)$$

to project the pions onto specific momentum states, we require the all-to-all propagator $S(t, \mathbf{z}; 0, \mathbf{x})$. This contains $12 \times 12 \times T \times L^3 \times L^3$ complex entries, and is actually a huge amount of information to construct. Nevertheless, we have proceeded to do this using stochastic sources, so that the propagator is given by

$$S(t, \mathbf{z}; 0, \mathbf{x}) \approx \frac{1}{N_r} \sum_{i=1}^{N_r} X_i(t, \mathbf{z}) \eta_i^*(\mathbf{x}) \quad (7.3)$$

where X is the solution vector and η is the random source vector (we use Z_2 noise); N_r is the number of random sources used. In the diagram, we have the option of using two sets of random sources, one for $S(t, \mathbf{z}; 0, \mathbf{x})$ and one for $S^\dagger(t, \mathbf{z}; 0, \mathbf{x})$, or we can use one set for both. In the latter case, there will be some correlation between the two propagators that does not correspond to physics, but is an additional source of error. By comparing to the point propagator calculation (only possible on very small lattices—which is why in this preliminary study we restrict ourselves to $4^3 \times 8$ lattice volumes), we are able to quantify how this correlation effect feeds into the error in the correlation function. It will be seen that using the two sets of random sources produces a much smaller $1/\sqrt{N_r}$ stochastic error.

Fig. 2 shows the relative error in the connected part of Diagram 0, i.e.,

$$\sum_{\mathbf{x}, \mathbf{y}, \mathbf{z}} \langle \text{Tr} [S(t, \mathbf{y}; 0, \mathbf{0}) S^\dagger(t, \mathbf{y}; 0, \mathbf{0})] \text{Tr} [S(t, \mathbf{z}; 0, \mathbf{0}) S^\dagger(t, \mathbf{x}; 0, \mathbf{0})] \rangle \quad (7.4)$$

in the two approaches for 10^3 random sources. It can be seen that using two independent sets leads to a significantly reduced error. In Fig. 3 we show what happens when the number of random sources is increased to 2×10^4 . While both relative errors are greatly reduced, it is

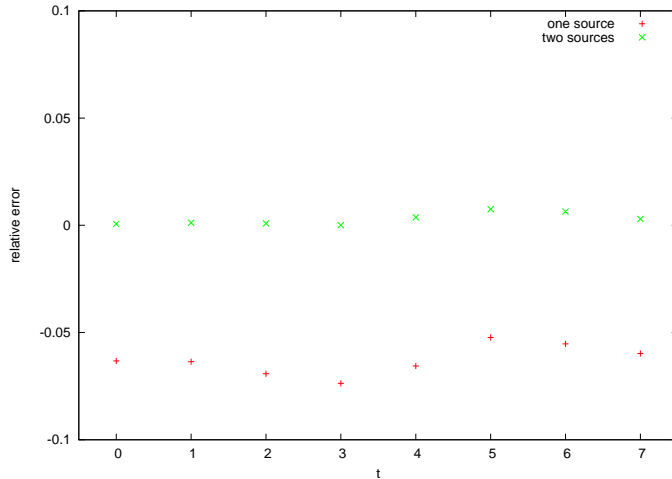


FIG. 2. Relative error using one set of 10^3 random sources for the two propagators versus two independent sets.

still the case that using two independent sets leads to a much smaller error. The main lesson of this part of our study is that stochastic error is much more efficiently reduced by using independent stochastic sources for each propagator than by merely increasing the number of sources but using the same set for each propagator.

In Table I we show timing benchmarks for computing C_0 on $4^3 \times 8$ and $8^3 \times 16$ lattices. The entry “ S_s fill” corresponds to the computation (7.3), which involves $288 \times L^7$ complex multiplications. “ S_s^\dagger fill” also includes the dagger operation. It can be seen that on the smaller lattice, it is still the inversion which takes the most time, but on the larger lattice, the fill operations are beginning to overwhelm the inversion. This is because the inversions scale as L^4 whereas the fill operations scale as L^7 . Note that for the inversions we are using QUDA [40], interfaced to the Columbia Physics System (CPS). We found that writing this interface was fairly simple to do and just involved some reordering of the arrays between the two libraries. We have only done this for clover fermions and our interface code is available upon request.

In order to partially overcome this problem, we have accelerated the fill operations by moving them to the GPU, which is an extension beyond simply using QUDA. This is straightforward to do and Table II shows the results. It can be seen that there is a speed-up of

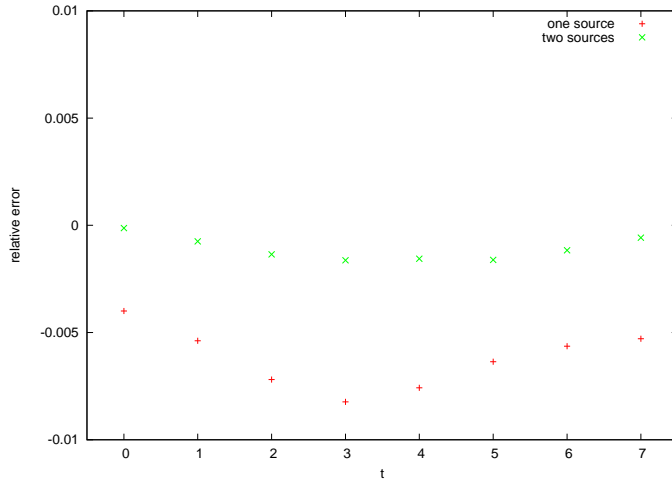


FIG. 3. Relative error using one set of 2×10^4 random sources for the two propagators versus two independent sets.

operation	$L = 4$ time (sec.)	$L = 8$ time (sec.)
inversion	0.519	8.8
S_s fill	0.185	17.4
S_s^\dagger fill	0.315	83.4
$\sum_y \text{Tr } S_p S_p^\dagger$	0.003	0.047
$\sum_x \sum_z \text{Tr } S_s S_s^\dagger$	0.190	43.3

TABLE I. Comparison of operational times for the $4^3 \times 8$ and $8^3 \times 16$ lattices. To get the total times per gauge field configuration, one should multiply the first three operations by N_r , and the last two operations by $T = 2L$. S_s is a stochastic propagator and S_p is a point source propagator. If S_s and S_s^\dagger use independent sets of random source vectors, in order to reduce error as explained in the text, then the inversion time should be multiplied by 2.

11.5 \times , and that the fill operation has now been brought to a level comparable to the inversion on the $L = 8$ lattice. However, increasing L will resurrect the problem, because of the poor scaling.

The origin of the undesirable L^7 scaling is the outer product operation (7.3). However,

operation	CPU time (sec.)	GPU time (sec.)	speed-up
S and S^\dagger fill	100.8	8.8	11.5

TABLE II. Comparison of time taken to fill the arrays of the stochastic propagators on the CPU versus the GPU. This is for an $L = 8$ lattice.

there is another method for dealing with stochastic propagators which avoids this outer product and only has an L^3 scaling.⁴ It is most easily illustrated by considering the single pion correlation function, projected to zero momentum. One simply rearranges the terms as follows:

$$\begin{aligned}
C(t - t_0) &= \left\langle \sum_{\mathbf{x}, \mathbf{y}} \text{Tr} [S(t_0, \mathbf{x}; t, \mathbf{y}) \gamma_5 S(t, \mathbf{y}; t_0, \mathbf{x}) \gamma_5] \right\rangle \\
&= \left\langle \frac{1}{N_r^2} \sum_{ij} \sum_{\mathbf{x}, \mathbf{y}} \text{Tr} [X_i(\mathbf{x}) \eta_i^*(\mathbf{y}) \gamma_5 X_j(\mathbf{y}) \eta_j^*(\mathbf{x}) \gamma_5] \right\rangle \\
&= \left\langle \frac{1}{N_r^2} \sum_{ij} \text{Tr} \left[\left(\sum_{\mathbf{y}} \eta_i^*(\mathbf{y}) \gamma_5 X_j(\mathbf{y}) \right) \left(\sum_{\mathbf{x}} \eta_j^*(\mathbf{x}) \gamma_5 X_i(\mathbf{x}) \right) \right] \right\rangle \quad (7.5)
\end{aligned}$$

Here, the i th random source is located on the timeslice t , and the j th random source is located on the timeslice t_0 . X_i and X_j are the respective solution vectors. What can be noticed in the final step is that the terms in parentheses do not involve $L^3 \times L^3$ outer products on each timeslice, but rather L^3 operations on each of the N_r^2 pairs i, j :

$$O_{ij}(t) = \sum_{\mathbf{y}} \eta_i^*(\mathbf{y}) \gamma_5 X_j(\mathbf{y}), \quad O_{ji}(t_0) = \sum_{\mathbf{x}} \eta_j^*(\mathbf{x}) \gamma_5 X_i(\mathbf{x}) \quad (7.6)$$

For the first operator, this must be carried out on each timeslice t , leading to another factor of $T = 2L$. Thus to form all of the $O_{ij}(t)$ requires $\mathcal{O}(N_r^2 L^4)$ floating point operations. The correlation function just involves i, j “contractions” of these “operators,”

$$C(t - t_0) = \frac{1}{N_r^2} \sum_{ij} \text{Tr} [O_{ij}(t) O_{ji}(t_0)] \quad (7.7)$$

This involves $\mathcal{O}(N_r^2)$ operations, which is quite large in our case where we have $N_r = 10^3$ due to the fact that we do not use any variance reduction techniques such as dilution (other than time-spin-color dilution). This approach is easily generalized to all of the diagrams in Fig. 1.

⁴ We thank Evan Weinberg for pointing this out to us.

The $\mathcal{O}(N_r^2 L^4)$ operations of this stochastic operator approach (i.e., forming $O_{ij}(t)$ in (7.6)) is to be compared with the $\mathcal{O}(L^7)$ operations in (7.3). The present method only becomes competitive when $L^3 \gtrsim N_r^2$, or for $L \gtrsim N_r^{2/3}$. Since we find that $N_r = 10^3$ is necessary in the absence of variance reduction techniques, this stochastic operator method does not become useful until $L \approx 100$. However, if dilution was used and N_r could be reduced to $N_r = 100$, then the present method begins to be more efficient when $L \geq 22$.

For the volumes that we consider in this paper, the prior method, which uses the outer product (7.3) is vastly more efficient since it avoids the factors of $N_r^2 = 10^6$. Once dilution is implemented in our future work, and for $L = 24$ and above, the stochastic operator method will become the preferred method.

VIII. CORRELATION FUNCTION

We have already given the expression for Diagram 0. Diagram 1 becomes

$$C_1(t, \mathbf{x}, \mathbf{y}, \mathbf{z}) = \left\langle \left(\text{Tr} [S(t, \mathbf{z}; t, \mathbf{y}) S^\dagger(t, \mathbf{z}; t, \mathbf{y})] - \langle \text{Tr} [S(t, \mathbf{z}; t, \mathbf{y}) S^\dagger(t, \mathbf{z}; t, \mathbf{y})] \rangle \right) \right. \\ \left. \times \left(\text{Tr} [S(0, \mathbf{x}; 0, \mathbf{0}) S^\dagger(0, \mathbf{x}; 0, \mathbf{0})] - \langle \text{Tr} [S(0, \mathbf{x}; 0, \mathbf{0}) S^\dagger(0, \mathbf{x}; 0, \mathbf{0})] \rangle \right) \right\rangle \quad (8.1)$$

Thus stochastic propagators must be calculated with the source at \mathbf{y} and the sink at \mathbf{z} . A few remarks about the subtraction of vacuum expectation values is in order. The operator $\pi^+ \pi^-$ has the same quantum numbers as the vacuum, so we must subtract off this piece. When we go to momentum space, this will only affect the zero momentum projection. A similar subtraction was necessary in the study [14] which used the interpolating operator $\sigma = \bar{q}q$. There they had to calculate $\langle (\sigma(t) - \langle \sigma \rangle)(\sigma(0) - \langle \sigma \rangle) \rangle$. Because they used Wilson fermions, they had to fight a battle with the enormous lattice artifacts in the Wilson fermion chiral condensate, $\langle \sigma \rangle \sim 1/a^3$. This resulted in a signal that was 1 part in 10^5 compared to the magnitudes of the quantities entering the subtraction. Of course this requires very large statistics in order to get a signal above the noise. We have a similar situation, with a signal that is 1 part in 10^4 compared to the quantities entering the subtraction. This is the most significant source of error in our calculation.

Diagram 2 is given by

$$C_2(t, \mathbf{x}, \mathbf{y}, \mathbf{z}) = \left\langle \text{Tr} [S^\dagger(0, \mathbf{x}; 0, \mathbf{0}) S(0, \mathbf{x}; t, \mathbf{z}) S^\dagger(t, \mathbf{y}; t, \mathbf{z}) S(t, \mathbf{y}; 0, \mathbf{0})] \right\rangle \quad (8.2)$$

Thus point propagators sourced at the origin can be used for $S^\dagger(0, \mathbf{x}; 0, \mathbf{0})$ and $S(t, \mathbf{y}; 0, \mathbf{0})$, whereas stochastic propagators sourced at (t, \mathbf{z}) are used for $S(0, \mathbf{x}; t, \mathbf{z})$ and $S^\dagger(t, \mathbf{y}; t, \mathbf{z})$.

Diagram 3 is the complex conjugate of Diagram 2. Since the total correlation function is the sum of the two, it suffices to take twice the real part of Diagram 2.

In Figs. 4-7 we show the results for each of the four diagrams, projected to zero momentum, for the lattice parameters that we have investigated. These are $\beta = 5.96$, corresponding to $a = 0.51 \text{ GeV}^{-1}$ [41], bare mass $m_0 a = -0.300$ corresponding to a pion mass of $m_\pi a \approx 1.0$ or $m_\pi \approx 2 \text{ GeV}$, and a lattice size of $L/a = 4 (4^3 \times 8)$. Note that we are using clover fermions with tree-level improved clover coefficient $c_{SW} = 1.0$, for an approximately $\mathcal{O}(a)$ improved formulation. For the size of lattice that we are using, with the lattice spacing of $a = 0.51 \text{ GeV}^{-1}$ the theory is well into the deconfined phase. To avoid this would require a significantly larger lattice, but here we are mostly just interested in the relative strengths of the four diagrams, the sizes of errors, and the lattice methods. So for our present purposes, being in the deconfined phase is not very important, though it does mean that the physical interpretation has to be one in terms of a high “temperature” limit. (Note however that since we have used periodic boundary conditions, the size in the temporal direction does not properly have an interpretation in terms of inverse temperature.) In Fig. 8 we show the sum of the diagrams,

$$C(t) = C_0(t) + C_1(t) - C_2(t) - C_3(t) \quad (8.3)$$

where the minus signs come from the fermion anticommutation in making the contractions.

For each of the diagrams, and for the sum of diagrams, we have extracted an effective mass, by fitting $C(t) = A \cosh[m_{\text{eff}}((T/2) - t)]$. It is interesting to see the behaviors in each of the channels. In particular, Diagram 1 is very flat and greatly lowers the effective mass of the total correlation function because of its large contribution to the overall result. However, we caution that not too much should be read into the masses that are obtained in this exploratory study, because of the very small lattice that is being used. The important take-away is the relative contribution of each diagram, and the importance of including all contractions. We anticipate that the qualitative features will be present also on larger lattices.

An important result of our study is the apportionment of the errors between the different diagrams. In the point source calculation, the error is entirely from having a finite sample

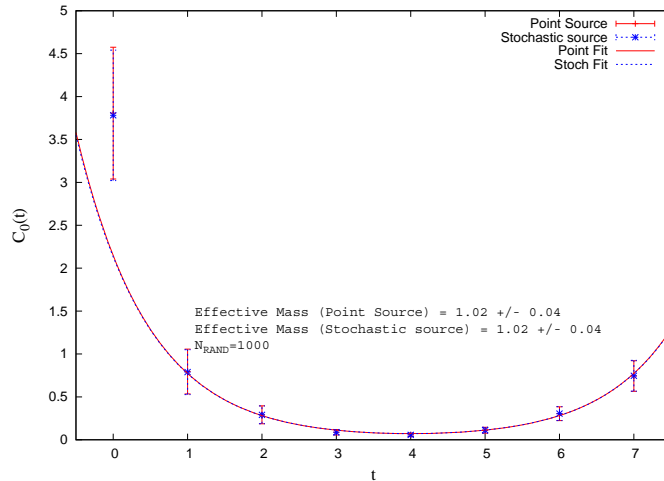


FIG. 4. Diagram 0, the correlation function $C_0(t)$, evaluated with all pseudoscalar operators except the one at the origin projected to zero momentum. Shown are results with both all-to-all propagators derived from point source inversions (exact) and all-to-all propagators derived from stochastic source inversions (approximate). Here, two stochastic propagators are obtained, each one using 10^3 random sources. It can be seen that the two methods are in excellent agreement. The effective mass for this diagram alone is relatively large, though significantly smaller than $2m_\pi$.

of gauge field configurations (100 in this study). This “gauge error” is displayed in Fig. 9, and it can be seen that the error budget is dominated by Diagram 1. This is to be expected, since it is completely disconnected at the quark level, and such diagrams are known to be quite noisy. It shows that the calculation of the full set of diagrams, including all of the disconnected contributions, is challenging and requires large statistics in order to obtain precise numbers. However, we find it encouraging that with a relatively small sample we are still able to extract a signal in Diagram 1. Fig. 10 shows the errors for each diagram coming from the stochastic calculation, obtained by comparing to the point source calculation. It can be seen that once again, the error in Diagram 1 dominates. It should also be noted that the error in Diagram 1 is amplified because of the vacuum subtractions. This is because the net result is the difference between two large quantities, each of which has a significant relative error.

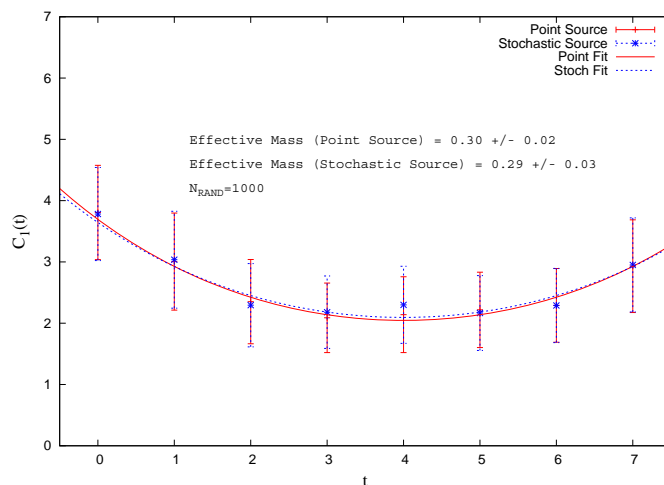


FIG. 5. Similar to Fig. 4, except for Diagram 1, $C_1(t)$. It can be seen that for this diagram, which has a gluonic intermediate state, the decay is quite shallow and the effective mass is small. This is likely an indication of the deconfined phase for the gluonic degrees of freedom. This diagram plays a very important role in the sum of diagrams, indicating that the lowest state has a large gluonic component.

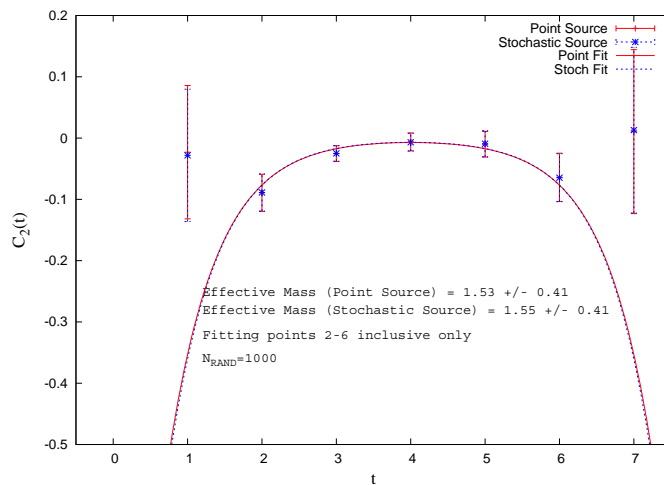


FIG. 6. Similar to Fig. 4, except for Diagram 2, $C_2(t)$. The values at $t = 0, 1, 7$ reflect the violation of unitarity in the quenched approximation, and are not included in the fit.

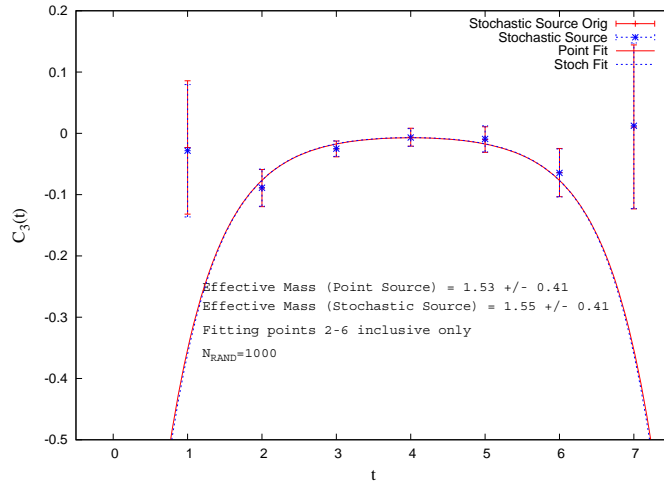


FIG. 7. Similar to Fig. 4, except for Diagram 3, $C_3(t)$. This diagram should be equal to $C_2(t)$ and comparing to Fig. 6 it can be seen that this is true within errors.

The effective mass derived from Fig. 8 is significantly smaller than the pion mass, which on these lattices is 1.67 ± 0.04 using the same cosh fit. This shows the large effect of Diagram 1 on the result. It is likely that this is due to gluonic configurations in the intermediate state being in the deconfined phase due to our very small volume. It seems that the lightest scalar state has a large gluonic component and that it is light because the infinite volume state is disintegrating. Sometimes it is stated that the $q\bar{q}$ and $q^2\bar{q}^2$ cannot mix with the glueball states in the quenched theory. This line of reasoning seems to arise from the fact that the glueballs are eigenstates of the Hamiltonian of the pure Yang-Mills theory, so they should be orthogonal to the states with quarks. However, the quenched theory is not unitary and so there is no reason to expect eigenstates to be orthogonal, since the full non-unitary theory does not have a Hermitian Hamiltonian. Thus we do not believe it is inconsistent to interpret Diagram 1 as being sensitive to mixing with gluonic states.

We observe violations of unitarity in our quenched simulation results, as is to be expected. This manifests itself as large negative contributions to the total correlation function $C(t)$ at time $t = 0$. These come from Diagrams 2 and 3, and are expected to disappear in an unquenched calculation. As a result of this unphysical feature, we do not include the $t = 0$ point in our fits.

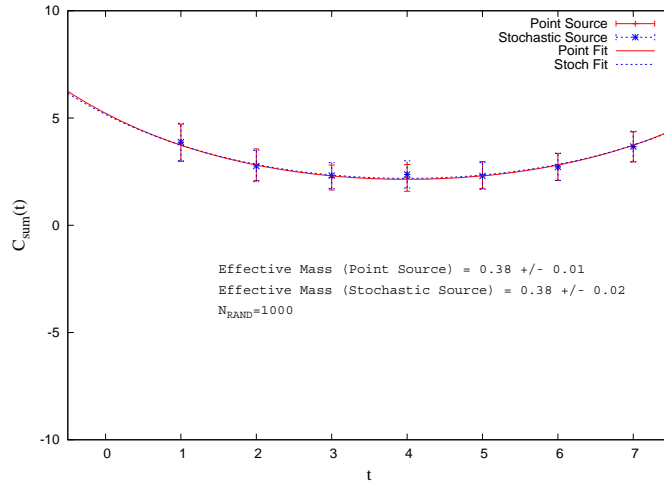


FIG. 8. Sum of the four diagrams, with appropriate minus signs. It can be seen that Diagram 1 has pulled the result for the effective mass down significantly.

IX. CONCLUSIONS

In this paper we have laid some ground work for a very demanding calculation, which consists of the extraction of the sigma resonance from lattice QCD. This is also relevant for the hunt for a techni-dilaton in nearly conformal theories. To do this properly, one must include contractions of the quark fields which require all-to-all propagators. These are particularly important for picking up the mixing between two-quark, four-quark and gluonic states.

While we find favorable results for using stochastic propagators in this calculation, it is interesting to also consider performing Fourier transforms “automatically” by using momentum source propagators. In the future we will repeat the present analysis on larger lattices using this technique. We will also be able to reduce the effective “temperature” (by increasing the size of the lattice) and see how the mixing of different components changes as this parameter is varied. Our results show that Diagram 1, the completely quark-disconnected diagram, can have a very strong impact on the estimate of the lightest scalar state, and that ignoring it would greatly change the results. This shows that a full treatment of all diagrams is essential for properly estimating the mass of the scalar ground state. We will

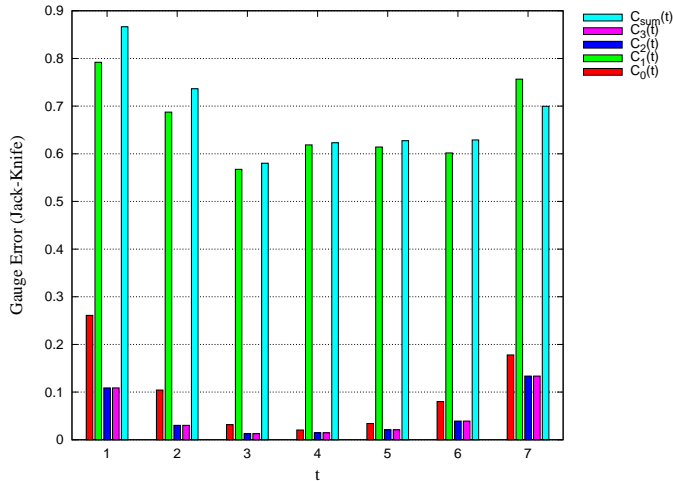


FIG. 9. Error budget from each of the diagrams, as well as the total, coming from having a finite number of gauge field configurations.

also in the future examine how our results change once dynamical fermions are included. We expect that Diagram 1 will continue to be important, but may become less dominated by gluonic states once quark loops are incorporated. It is also worth noting the results of Ref. [42], which indicate that Diagrams 2 and 3 are quite important to the states we are considering. In any event, both our empirical results and the analytical methods of Ref. [42] raise serious questions about previous studies that ignored such diagrams.

Once we have obtained data for a variety of L , we will be able to extract the scattering phase shift $\delta(s)$. As mentioned in our discussion above, this data should then be fitted to analytic forms, as has been done with the experimental data in [38]. These analytic forms then allow for the determination of the pole location in a straightforward manner. Hopefully there will be a concordance with results obtained from interpolating operators, subtracting out the scattering states.

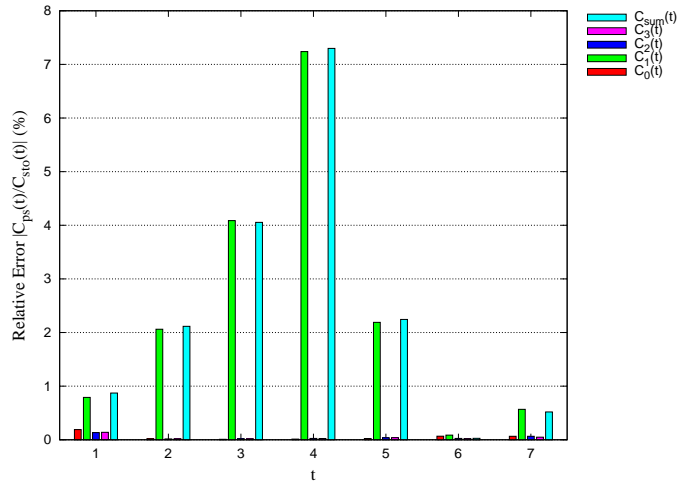


FIG. 10. Error budget from each of the diagrams, as well as the total, according our estimate of stochastic error.

ACKNOWLEDGEMENTS

We wish to thank Keh-Fei Liu and Evan Weinberg for helpful discussions. D.H. was supported in part by NSF Grant No. PHY-1212272.

-
- [1] Z. Fodor, K. Holland, J. Kuti, D. Nogradi, C. Schroeder, *et al.*, Phys.Lett. **B718**, 657 (2012), arXiv:1209.0391 [hep-lat].
 - [2] D. D. Dietrich, F. Sannino, and K. Tuominen, Phys.Rev. **D72**, 055001 (2005), arXiv:hep-ph/0505059 [hep-ph].
 - [3] K. Yamawaki, Int.J.Mod.Phys. **A25**, 5128 (2010), arXiv:1008.1834 [hep-ph].
 - [4] R. Foadi, M. T. Frandsen, and F. Sannino, Phys.Rev. **D87**, 095001 (2013), arXiv:1211.1083 [hep-ph].
 - [5] R. L. Jaffe, Phys.Rev. **D15**, 267 (1977).
 - [6] R. L. Jaffe, Phys.Rev. **D15**, 281 (1977).
 - [7] C. Michael, Nucl.Phys. **B327**, 515 (1989).
 - [8] T. A. DeGrand, Phys.Rev. **D43**, 2296 (1991).

- [9] C. McNeile, *Int.Rev.Nucl.Phys.* (2003), arXiv:hep-lat/0307027 [hep-lat].
- [10] C. E. Detar and J. B. Kogut, *Phys.Rev.* **D36**, 2828 (1987).
- [11] M. G. Alford and R. Jaffe, *Nucl.Phys.* **B578**, 367 (2000), arXiv:hep-lat/0001023 [hep-lat].
- [12] W.-J. Lee and D. Weingarten, *Phys.Rev.* **D61**, 014015 (2000), arXiv:hep-lat/9910008 [hep-lat].
- [13] C. McNeile and C. Michael (UKQCD Collaboration), *Phys.Rev.* **D63**, 114503 (2001), arXiv:hep-lat/0010019 [hep-lat].
- [14] T. Kunihiro *et al.* (SCALAR Collaboration), *Phys.Rev.* **D70**, 034504 (2004), arXiv:hep-ph/0310312 [hep-ph].
- [15] A. Hart, C. McNeile, C. Michael, and J. Pickavance (UKQCD Collaboration), *Phys.Rev.* **D74**, 114504 (2006), arXiv:hep-lat/0608026 [hep-lat].
- [16] N. Mathur, A. Alexandru, Y. Chen, S. Dong, T. Draper, *et al.*, *Phys.Rev.* **D76**, 114505 (2007), arXiv:hep-ph/0607110 [hep-ph].
- [17] N. Mathur, F. Lee, A. Alexandru, C. Bennhold, Y. Chen, *et al.*, *Phys.Rev.* **D70**, 074508 (2004), arXiv:hep-ph/0406196 [hep-ph].
- [18] K.-F. Liu, *Prog.Theor.Phys.Suppl.* **168**, 160 (2007), arXiv:0706.1262 [hep-ph].
- [19] S. Prelovsek and D. Mohler, *Phys.Rev.* **D79**, 014503 (2009), arXiv:0810.1759 [hep-lat].
- [20] S. Prelovsek, T. Draper, C. B. Lang, M. Limmer, K.-F. Liu, *et al.*, *Phys.Rev.* **D82**, 094507 (2010), arXiv:1005.0948 [hep-lat].
- [21] H. Suganuma, K. Tsumura, N. Ishii, and F. Okiharu, *Prog.Theor.Phys.Suppl.* **168**, 168 (2007), arXiv:0707.3309 [hep-lat].
- [22] M. Loan, Z.-H. Luo, and Y.-Y. Lam, *Eur.Phys.J.* **C57**, 579 (2008), arXiv:0907.3609 [hep-lat].
- [23] M. Wakayama and C. Nonaka, *PoS LATTICE2012*, 276 (2012), arXiv:1211.2072 [hep-lat].
- [24] M. Wakayama, *PoS Hadron2013*, 106 (2014).
- [25] M. Luscher, *Commun.Math.Phys.* **104**, 177 (1986).
- [26] M. Luscher, *Commun.Math.Phys.* **105**, 153 (1986).
- [27] M. Luscher, *Nucl.Phys.* **B354**, 531 (1991).
- [28] M. Luscher, *Nucl.Phys.* **B364**, 237 (1991).
- [29] K. Rummukainen and S. A. Gottlieb, *Nucl.Phys.* **B450**, 397 (1995), arXiv:hep-lat/9503028 [hep-lat].
- [30] S. Prelovsek, C. Lang, and D. Mohler, (2011), presented at Bled Mini-Workshop 2011, 3-10 July, Bled, Slovenia, arXiv:1110.4520 [hep-ph].

- [31] C. Lang, D. Mohler, S. Prelovsek, and M. Vidmar, Phys.Rev. **D84**, 054503 (2011), arXiv:1105.5636 [hep-lat].
- [32] S. Prelovsek, C. Lang, D. Mohler, and M. Vidmar, (2011), arXiv:1111.0409 [hep-lat].
- [33] N. Ishizuka for PACS-CS Collaboration, PoS **LATTICE2011**, 125 (2011), arXiv:1111.0377 [hep-lat].
- [34] S.R. Beane, E. Chang, W. Detmold, H.W. Lin, T.C. Luu, K. Orginos, A. Parreno, M.J. Savage, A. Torok, A. Walker-Loud, (2011), arXiv:1107.5023 [hep-lat].
- [35] S.Aoki, K.I.Ishikawa, N.Ishizuka, K.Kanaya, Y.Kuramashi, Y.Namekawa, M.Okawa, Y.Taniguchi, A.Ukawa, N.Ukita, T.Yamazaki, T.Yoshié, (2011), arXiv:1106.5365 [hep-lat].
- [36] Z. Fu, (2011), arXiv:1110.5975 [hep-lat].
- [37] J. Nebreda and J. Pelaez., Phys.Rev. **D81**, 054035 (2010), arXiv:1001.5237 [hep-ph].
- [38] I. Caprini, Phys.Rev. **D77**, 114019 (2008), arXiv:0804.3504 [hep-ph].
- [39] L. Y. Glozman, C. Lang, and M. Limmer, Phys.Rev.Lett. **103**, 121601 (2009), arXiv:0905.0811 [hep-lat].
- [40] R. Babich, K. Barros, R. Brower, M. Clark, J. Giedt, S. Gottlieb, B. Joó, C. Rebbi, G. Shi, and A. Strelchenko, [Http://lattice.github.com/quda](http://lattice.github.com/quda).
- [41] M. Guagnelli, R. Sommer, and H. Wittig (ALPHA collaboration), Nucl.Phys. **B535**, 389 (1998), arXiv:hep-lat/9806005 [hep-lat].
- [42] F.-K. Guo, L. Liu, U.-G. Meissner, and P. Wang, Phys.Rev. **D88**, 074506 (2013), arXiv:1308.2545 [hep-lat].